Published in final edited form as:
Biochemistry. 2010 March 2; 49(8): 1649–1657. doi:10.1021/bi902084y.

Comparison of binding platforms yields insights into receptor binding differences between Shiga toxins 1 and 2[†]

Michael J. Flagler[‡], **Sujit S. Mahajan**[§], **Ashish A. Kulkarni**[§], **Suri S. Iyer**[§], and **Alison A. Weiss**[*,‡]

[‡]Department of Molecular Genetics, Biochemistry and Microbiology, University of Cincinnati, Cincinnati, OH 45267

[§]Department of Chemistry, University of Cincinnati, Cincinnati, OH 45221

Abstract

Protein-glycan interactions are typically very weak, and avid binding is achieved when proteins express multiple glycan binding sites. Shiga toxin (Stx) uses glycan receptors to enter cells. Stx has five identical binding subunits, each with three non-identical glycan binding sites. Previous studies examined binding to biantennary glycans expressing Pk trisaccharide mimics immobilized on streptavidin, resulting in display of four trisaccharides per streptavidin face. Stx1 preferred the Pk trisaccharide of its native receptor, globotriaosylceramide (Gb3), while the more potent and clinically relevant variant, Stx2, preferred the Pk trisaccharide with the terminal galactose replaced with N-acetyl galactosamine (NHAc-Pk). In the present study, binding of Stxs to Pk analogues was examined using two experimental platforms, ELISA and surface plasmon resonance (SPR). ELISA was more sensitive than SPR. Sensitivity in the ELISA was due to high streptavidin density, suggesting that avid binding may require engagement of more than four trisaccharides. Selectivity for the Pk analogues was maintained in both experimental platforms. Glycan preference was mapped to binding site 2, since reciprocal mutation of a single amino acid (asparagine 32 of Stx1 B-subunit / serine 31 of Stx2 B-subunit) reversed binding preference. However, native Stx1 bound well to plates loaded with a 50:50 mixture of Pk:NHAc-Pk, while Stx2 bound less efficiently, suggesting that one of the Stx1 binding sites may only engage Pk, while another may tolerate either Pk or NHAc-Pk. Varying glycan structure and density across different *in vitro* binding platforms revealed important differences in receptor binding properties between Stx1 and Stx2.

Disease caused by the Gram-negative pathogen *Escherichia coli* O157:H7 can progress to the life-threatening sequela hemolytic uremic syndrome (HUS), the most common cause of acute renal failure in children (1). In the United States alone, *E. coli* O157:H7 accounts for an estimated 110,000 cases of disease, 3,200 hospitalizations, and more than 60 deaths annually (2). Treatment of *E. coli* O157:H7 illness is complicated by the fact that antibiotic treatment enhances disease progression (3). To date, there are no post-exposure therapeutics available for the treatment of *E. coli* O157:H7 infection.

The pathogenicity of *E. coli* O157:H7 is linked to the production of one or more members of the Shiga toxin (Stx) family of bacterial toxins. Stx is an AB_5 toxin (4). The A-subunit

[†]This work was supported by National Institutes of Health Grants R01 AI 064893 (A.A.W.), U01 AI 075498 (A.A.W. and S.S.I.), and NSF CAREER CHE-0845005 (S.S.I.).

[*]To whom correspondence should be addressed. A.A.W.: Department of Molecular Genetics, Biochemistry and Microbiology, University of Cincinnati, 231 Albert Sabin Way, Cincinnati, OH 45267-0524; phone, (513) 558-2820; fax, (513) 558-8474; Alison.Weiss@uc.edu.

possesses RNA N-glycohydrolase activity and mediates host cell damage by cleaving a nucleotide from the 28S ribosomal RNA, inhibiting protein synthesis (5). The A-subunit is delivered into the cell by a ring-like structure comprised of five identical B-subunits that bind to carbohydrate receptors on the cell surface (6).

The Stx family consists of two antigenically distinct toxins, Stx1 and Stx2, which share 55% and 57% amino acid homology in the A- and B-subunits, respectively (7). The lethal dose of Stx2 is approximately 400-fold lower than that of Stx1 in the mouse model (8), and the vast majority of fatal human disease cases result from Stx2-producing *E. coli* strains (9). The basis for the difference in potency between Stx1 and Stx2 is unknown. Furthermore, a number of variants of Stx2 exist (subtypes Stx2b-2g) (10), and emerging epidemiological evidence suggests that different Stx2 subtypes may be associated with different disease outcomes (11). For example, the glycolipid globotriaosylceramide (Gb3) has been well-characterized as a receptor for Stx1 (12-16), with the terminal Pk trisaccharide serving as the major receptor binding site. Stx2e, a variant of Stx2 which binds preferentially to the glycolipid globotetraosylceramide (Gb4) as opposed to Gb3 (17), is associated with mild disease in humans (18) but causes edema disease in piglets (19). Receptor binding differences between Stx1 and Stx2 have been hypothesized to play an important role in mediating the difference in potency (20). Toxicity studies with Stx A/B-subunit chimeras suggest that the B-subunit plays a critical role in mediating Stx potency (21-23). Interestingly, despite exhibiting a lower potency *in vivo*, binding studies have demonstrated that Stx1 binds with higher affinity than Stx2 to the Pk trisaccharide (24) and Gb3 receptor mimics (21,25).

The majority of protein-monosaccharide interactions exhibit low intrinsic affinities (26) and multivalency is therefore required to achieve tight binding. Numerous examples exist in which nature exploits multivalent interactions between proteins and carbohydrates to elicit biological responses (27), a phenomenon which has been termed the glycoside cluster effect (26,27). Multivalent interactions have been shown to be important in Stx binding. Univalent binding of the Stx1 B-subunit (Stx1B) to the Pk trisaccharide was shown to be very weak by isothermal microcalorimetry, exhibiting a 0.5-1 mM dissociation constant (K_d) for B-subunit monomer (28). In contrast, binding of Stx1 and Stx2 to Gb3 in lipid layers designed to mimic the cell membrane surface and thereby facilitate multivalent interactions exhibited much higher affinities in both ELISA (21) and surface plasmon resonance (SPR) (29) studies. In one SPR study, the affinity for the interaction of Stx1B with Gb_3 incorporated into model membranes (K_d = 3.0 nM) was over 10^6-fold higher than that for univalent Pk trisaccharide in solution (K_d = 4.8 mM) (29).

The crystal structure of the Stx1 B-pentamer with bound Pk demonstrates the presence of three Pk binding sites, which have been named sites 1, 2, and 3 (30) (Figure 1A). Site 2 has been suggested to be the primary, high affinity binding site for Pk. This site showed the strongest electron density for Pk in the Stx1B/Pk crystal structure (30) and also exhibited the highest occupancy level of the Pk binding sites in an NMR solution structure of the Stx1 B-pentamer bound to Pk (31). In fact, in the Stx1B/Pk solution structure, occupancy at site 1 was less than 15% with respect to site 2, and no evidence could be found for binding at site 3 (31). Similar crystal structures are not available for Stx2.

Recently, we demonstrated that Stx2 exhibits different binding preferences from Stx1, and preferentially recognizes Pk with the terminal galactose modified by N-acetylation (32,33). In the present study, binding of Stx1 and Stx2 to synthetic Pk analogues was compared across two binding platforms, ELISA and SPR, both of which utilized streptavidin-biotin conjugation chemistry. The high affinity streptavidin-biotin interaction offers a simple, convenient method for immobilizing biotinylated molecules to streptavidin-coated surfaces.

Streptavidin is a tetrameric protein comprised of four 13 kDa subunits, each of which binds one molecule of biotin with extremely high affinity (K_d = ~10^{-15} M) (34). The biotin sites are located two per face of the streptavidin molecule at a distance of 20 Å apart. The constraints placed upon receptor presentation by this system enable a systematic and quantitative study of the effect of receptor density and presentation on complex, multivalent protein-carbohydrate interactions.

To better understand the parameters responsible for differences in receptor recognition by Stx1 and Stx2, a comparative analysis of Stx1 and Stx2 binding across different platforms, receptor densities, and glycan populations was performed. The results of this study provide important insight into the complex mechanisms underlying the differences in Stx1 and Stx2 receptor interactions.

MATERIALS AND METHODS

Protein expression and purification

pET21b(+) expression plasmids (Novagen, Darmstadt, Germany) encoding the Stx1 and Stx2 B-subunits were transformed into BL21(DE3)pLysS *E. coli* (Protein Express, Cincinnati, OH). Transformants were cultured in Luria-Bertani (LB) broth containing ampicillin (250 μg ml^{-1}) and chloramphenicol (34 μg ml^{-1}) at 37 °C, 250 rpm until reaching an OD_{600} value of 1. Cultures were cooled to 8 °C and B-subunit expression was induced with 0.1 mM IPTG and 2% ethanol, followed by shaking incubation for 16 h at 20 °C. Stx B-subunits were purified from induced culture lysates by ammonium sulfate precipitation, Q Sepharose™ Fast Flow ion exchange chromatography (GE Healthcare, Uppsala, Sweden) and Superdex™ 75 HiLoad 26/60 size exclusion chromatography (GE Healthcare). Stx1B underwent an additional purification step using Uno™ Q6R ion exchange chromatography (Bio-Rad, Hercules, CA). All column chromatography steps were performed using an ÄKTA FPLC system (GE Healthcare). Purity of the Stx B-subunits was verified by the presence of single band at 8 kDa on Coomassie-stained gels when 1 μg of protein was separated by sodium dodecyl sulfate-polyacrylamide gel electrophoresis (SDS-PAGE). Protein concentrations were determined using the Bicinchoninic Acid Protein Assay (Pierce, Rockford, IL). For studies requiring high concentrations of Stx holotoxin, culture supernatant containing unpurified holotoxin at about 200 μg ml^{-1} of toxin was used, as previously described (33). Holotoxin binding was also studied using purified recombinant toxoids of the Stx1 and Stx2 holotoxins containing genetic mutations in the catalytic A-subunit which render the proteins non-toxic without altering binding. The Stx toxoids were obtained from the Biodefense & Emerging Infections Resources Repository (Manassas, VA).

Glycoconjugates

Synthesis of the Pk glycoconjugates used in this study has been described previously (33). The Pk glycoconjugates were comprised of trisccharides attached to a biotinylated dimeric scaffold via a six carbon spacer (Figure 2A and B). The recognition elements consist of either the trisaccharide moiety of Pk (Galα1-4Galβ1-4Glc) or a modified form of Pk which has an N-acetyl group in place of the hydroxyl group on carbon 2 of the terminal galactose (GalNacα1-4Galβ1-4Glc). The mannose glycoconjugate was comprised of mannose attached to a biotinylated monomeric scaffold via a six carbon spacer (Figure S1 of the Supporting Information). Biotinylated polyethylene glycol (PEG, MW 3400) was purchased from Laysan Bio (Arab, AL).

Surface plasmon resonance (SPR)

Binding of Stx B-subunits to Pk analogues was measured using a BIAcore 2000 instrument (GE Healthcare). Biotinylated glycoconjugates were injected over streptavidin coated SA sensor chips (GE Healthcare) at 10 μl min^{-1} until saturation was achieved. A reference flow cell was used to record the background response and background was subtracted from each sample. Biotinylated PEG 3400 was used as the reference. The running buffer used in all experiments was 100 mM HEPES, 100 mM NaCl, 3 mM EDTA, pH 7.4. All SPR experiments were performed at room temperature. Stx holotoxins and B-subunits were injected over the chip at 10 μl min^{-1} for 3.5 min. Binding was detected as a change in the refractive index at the surface of the chip as measured by response units (RU). Data analysis was carried out using BIAevaluation 3.0 Software.

Enzyme-linked immunosorbent assays (ELISAs)

Binding of Stxs to Pk analogues was measured in Reacti-Bind™ Streptavidin High Binding Capacity Coated 96-Well Plates and Reacti-Bind™ Streptavidin Coated 96-Well Plates (Pierce), containing binding capacities of 125 pmol and 5 pmol D-biotin per well, respectively. All ELISA experiments were performed at room temperature. Wash steps were carried out in an EL_X 405 Auto Plate Washer (Bio-Tek Instruments, Winooski, VT) using PBS (8.1 mM Na_2HPO_4, 1.5 mM KH_2PO_4, 128 mM NaCl, 2.7 mM KCl) pH 7.4 containing 0.5% Tween 20 and 1 g L^{-1} BSA. Plates were blocked with wash buffer prior to immobilization of glycoconjugates to eliminate non-specific binding. Biotinylated glycoconjugates were immobilized in the ELISA wells, followed by 1 h incubation with Stx holotoxins or B-subunits, unless specified otherwise. Toxins were detected using rabbit polyclonal antibodies against Stx1 and Stx2 (Meridian Bioscience, Cincinnati, OH). Stx B-subunit binding was measured by colorimetric reaction using alkaline phosphatase-conjugated goat anti-rabbit IgG (Sigma-Aldrich, St. Louis, MO) and SIGMA *FAST*™ p-Nitrophenyl Phosphate Tablets (Sigma-Aldrich). Stx holotoxin binding was measured by fluorimetric reaction using peroxidase-conjugated goat anti-rabbit IgG (MP Biomedicals, Solon, OH) and QuantaBlu™ Fluorogenic Peroxidase Substrate (Pierce).

Determination of intramolecular and intermolecular distances

Distances between receptor binding sites in the Stx1 B-pentamer were determined from the crystal structure of the Stx1 B-pentamer with bound Pk (PDB ID: 1BOS) (30) using PyMOL™ v1.2 Software (DeLano Scientific, Palo Alto, CA). Carbon 6 of the penultimate galactose (Gal2) of the Pk trisaccharide bound at each site was used for measurements of inter-binding site distances, with the exception of binding sites in which only the terminal galactose (Gal1) was resolved. The distance between intramolecular biotin sites in streptavidin was determined from the crystal structure of core streptavidin (amino acid residues 13-139) bound to biotin (PDB ID: 1SWE) (35) using PyMOL v1.2 Software. The biotin atom which is conjugated to the linker element of the glycoconjugates used in this study was used as reference point to measure the distance between biotin molecules located on the same face of the streptavidin polypeptide. The average intermolecular distance between tetrameric streptavidin molecules in the SPR platform was derived mathematically. The streptavidin capacity of the BIAcore SA chip is 4000-6000 RU or 400-600 ng per cm^2 (1000 RU = 100 ng per cm^2) (36). The flow cell area on the SA sensor chip is 1.2 mm^2 ((37), and manufacturer correspondence) and the height of the dextran matrix is 50 nm (36). The molecular weight of tetrameric streptavidin (52.8 kDa), along with the information cited above, was used to calculate the distance between streptavidin molecules assuming homogeneous distribution of the streptavidin molecules in three-dimensional space.

RESULTS

Binding of Stxs to Pk analogues in SPR platform

To compare the interactions of Stxs with Pk analogues across different binding platforms, binding of purified Stx1 and Stx2 B-subunits to synthetic glycoconjugates was measured by SPR. Biotinylated dimers of Pk (Figure 2A) and NHAc-Pk (Figure 2B) were immobilized on a streptavidin coated biosensor chip. Selective binding of Stx1B to Pk (Figure 2, red) and Stx2B to NHAc-Pk (Figure 2, blue) were observed, consistent with ELISA binding data for Stx1 and Stx2 holotoxins (33).

Binding of culture supernatant containing Stx1 and Stx2 holotoxins to Pk analogues in the SPR platform exhibited similar binding curves to the B-subunits (Figure 2A and B). Kitova et al. have reported that the Stx2 B-subunit exists predominantly as a pentamer only at high subunit concentrations, above 50μM (38), while the Stx1 and Stx2 holotoxin complexes are more stable (39). While differences in the stability of the Stx1 and Stx2 B-pentamers could influence binding, these results suggest that assembly state differences between the Stx B-pentamer and the holotoxin did not have a major influence on binding in this system.

Saturated binding was not achievable. Comparison of the sensograms for the Stx1B and Stx2B binding interactions revealed that binding of Stx1B to Pk occurred with noticeably slower on/off kinetics than binding of Stx2B to NHAc-Pk (Figure 3A, Figure S2 of the Supporting Information). Stx2B came unbound from NHAc-Pk almost immediately at the end of the injection, suggesting a weak interaction with NHAc-Pk in this system. In contrast, Stx1B binding to Pk was detected for over 3 min following the end of injection, suggesting that a stronger interaction had occurred. First-order plots of the kinetics of dissociation using the methods of Winzor (40) suggest that multivalent binding occurred for both Stx1B to Pk and Stx2B to NHAc-Pk in the SPR platform (Figure 3B and C). However, the rapid association kinetics of association and dissociation for both the Stx1B and Stx2B binding interactions preclude fitting the data to mathematical models.

Comparison of Stx binding in ELISA and SPR platforms

Binding of purified, genetically-inactivated Stx holotoxins and B-subunits were tested in a high-binding capacity ELISA platform, in which biotinylated Pk analogues were immobilized in streptavidin coated 96-well plates. Binding of Stx1 and Stx2 in the ELISA platform using high-binding capacity streptavidin plates (Figure 2A and B, black symbols) was compared to the SPR platform. The high-binding capacity ELISA platform was several orders of magnitude more sensitive than the SPR platform for detecting Stx binding.

Protein-glycan contact time has been shown to play a critical role in the establishment of binding interactions in other systems (41). The effect of incubating the toxins with Pk analogues under static (ELISA) vs. dynamic flow (SPR) conditions could have contributed to the difference in sensitivity of the two platforms, since the short incubation time under continuous flow in the SPR platform could prohibit engagement of multiple binding sites in the toxin. In the ELISA, toxins were incubated in the wells for 1 h, whereas in the SPR, toxins were flowed over the surface of the sensor chip for 3.5 min at a flow rate of 10 μl min^{-1}. However, ELISA studies performed using a 30-sec incubation with toxin resulted in more than 50% of the binding observed for a 60 min incubation (Figure S3 of the Supporting Information), indicating that a strong binding interaction between Stxs and Pk analogues occurs very rapidly in the ELISA platform. Therefore, Stx-glycan contact time is not likely responsible for the difference in sensitivity between the ELISA and SPR platforms.

Effect of receptor density on Stx receptor binding

The effect of streptavidin density on Stx holotoxin binding to Pk analogues was measured on both high binding-capacity (125 pmol D-biotin capacity per well) and low binding-capacity (5 pmol D-biotin capacity per well) ELISA plates. As expected, less overall toxin binding was observed for the low binding-capacity ELISA plates (about 50% less for Stx1 and 70% less for Stx2 at the highest toxin concentration tested). To compare binding between the high and low binding-capacity plates, the data are plotted as % of the value obtained for the highest toxin concentration tested for each plate (Figure 4A). In the high binding-capacity ELISA, the global affinity of Stx1 for Pk (K_d = 1.4 nM) was about 50-fold greater than that of Stx2 for NHAc-Pk (K_d = 69.1 nM) (Figure 4A, Figure S4 of the Supporting Information). However, the global affinity of Stx1 for Pk was reduced by almost 100-fold in the low binding-capacity ELISA ($K_d \geq 137$ nM). In contrast, the global affinity of Stx2 for NHAc-Pk was nearly the same in the low binding-capacity ELISA (K_d= 106.4 nM) as the high binding-capacity ELISA (K_d= 69.1nM) (Figure 4A, Figure S4 of the Supporting Information). Therefore, although less overall binding was observed in the low binding-capacity ELISA, the interactions that occur between Stx2 and NHAc-Pk in the high and low binding-capacity ELISA platforms are likely the same. In contrast, the 100-fold difference in global affinity of Stx1 for Pk between the high and low binding-capacity ELISA platforms suggests that multivalent binding interactions that occur at high receptor density are unable to occur when receptor density is low.

In contrast to modulating the distance between receptor glycans by altering streptavidin density in the ELISA, the effect of receptor density on Stx binding was also tested in the high binding-capacity ELISA in a different manner by coating the wells with Pk analogues pre-mixed with different ratios of biotinylated PEG. In this manner, occupancy of the biotin sites of a single streptavidin were altered, and receptor density was diluted to 100, 75, 50, 25, 10 and 0% in the ELISA wells. Binding of Stx1 and Stx2 was assessed at 5 μg of toxin per well (0.66 μM), a concentration at which both Stx1 and Stx2 binding had reached saturation in the high binding-capacity ELISA (Figure 4A), and 1 μg of toxin per well (0.13 μM), and toxin concentration did not affect binding to the receptor dilutions. At 75% receptor density, binding of Stx1 to Pk was reduced by approximately 50%, whereas binding of Stx2 to NHAc-Pk was reduced by approximately 90% (Figure 4B). At receptor densities of 50% or less, very little binding of either Stx1 or Stx2 to their respective Pk analogues was observed.

Influence of heterogeneous glycan populations on Stx binding

Glycan arrays consisting of large numbers of homogeneous glycan targets covalently linked to glass surfaces have become important tools for screening of glycan-binding protein specificity. However, these arrays do not mimic the true heterogeneous surface of cells, and recent binding studies using combinatorial glycoarrays have demonstrated that the binding of bacterial toxins can be attenuated, enhanced, or unaffected in the presence of different glycolipid complexes (42). To determine whether the presence of other glycans can influence binding, binding of Stx1 and Stx2 at 1 μg of toxin per well (0.13 μM) was tested in the presence of 50:50 mixtures of various biotinylated glycoconjugates. Binding of Stx1 to Pk diluted 50:50 with NHAc-Pk, mannose, or PEG (MW 3400) was assessed (Figure 5, black bars), while NHAc-Pk, mannose, and PEG alone served as controls. Almost no binding occurred when Pk was diluted with mannose or PEG. However, 86% of binding of Stx1 to Pk alone was retained when Pk was diluted 50:50 with NHAc-Pk, even though no binding to NHAc-Pk alone was detected. These results suggest that NHAc-Pk can replace one of the Pk dimers if another Pk dimer is present, and thereby permit Stx1 binding. A reciprocal study was performed for Stx2, in which NHAc-Pk was diluted with Pk, Mannose, or PEG (Figure 5, white bars). Almost no binding of Stx2 occurred when NHAc-Pk was

diluted with mannose or PEG, or in the presence of Pk alone. However, 25% of binding of Stx2 to NHAc-Pk alone was retained when NHAc-Pk was diluted 50:50 with Pk, suggesting that substituting an NHAc-Pk dimer for a Pk dimer in the presence of NHAc-Pk allows some Stx2 binding to occur; however, binding of Stx2 to the 50:50 Pk / NHAc-Pk mixture was much less efficient than that of Stx1.

Receptor binding site 2 confers specificity toward Pk analogues

Binding site 2 of the Stx1 B-pentamer is the high affinity binding site for Pk (Figure 1A). If Stx2 utilizes site 2 to bind to NHAc-Pk, substitution of the corresponding amino acids from Stx1 may alter specificity. To test this hypothesis, a number of non-conserved amino acid pairs in binding sites were mutated, including D16/E15, F30/W29, N32/S31, N55/S54, and A56/T55 of Stx1 and Stx2, respectively. However, only N32 / S31 exchange reversed the binding preference for both Stx1 and Stx2 to Pk analogues, and only this mutant pair was characterized further. The Asn to Ser substitution resulted in improved binding of Stx1B to NHAc-Pk (Figure 6B and D, black squares), while decreasing binding to Pk (Figure 6 A and C, black squares), in either the ELISA or SPR platform. Likewise, the Ser to Asn substitution resulted in slight binding of Stx2B to Pk (Figure 6C, black circles), while completely abrogating binding to NHAc-Pk (Figure 6D, black circles) when examined using the SPR platform. Combined, these data suggest that site 2 is involved in the interactions of both Stx1 and Stx2 with the Pk analogues, and that the amino acid sequence at this site confers specificity.

DISCUSSION

In previous studies, we demonstrated that Stx1 and Stx2 bind selectively to different Pk analogues in an ELISA platform (33). In the current study, the scope of this work was extended to examine Stx binding to Pk analogues across different experimental platforms. Very few quantitative studies comparing ELISA and SPR have been performed. As an advantage over ELISA, binding in SPR is detected in real time, enabling measurement of on/off binding kinetics. Additionally, SPR is a label-free technique and no amplification using primary and secondary antibodies is required. While the dissociation kinetics for both Stx1B and Stx2B binding to Pk analogues in the SPR platform suggest that multivalent interactions occurred, slower on/off kinetics were observed for the Stx1B/Pk interaction than the Stx2B/NHAc-Pk interaction.

Even though streptavidin was used to immobilize in both platforms, ELISA was much more sensitive than SPR for the detection of Stxs. Each tetrameric streptavidin molecule contains four biotin sites; two of the biotin sites are located 20 Å apart on one face of the complex, while the other two are located the same distance apart on the opposite face. Due to size constraints, a single molecule of Stx can only engage biantennary glycans immobilized on two sites 20 Å apart (Figure 1A), implying that each streptavidin molecule affords the opportunity for Stx to engage up to four glycan binding sites. In the SPR platform, tetramers of streptavidin are amine-coupled to a negatively charged carboxymethylated dextran matrix on the surface of the sensor chip, and the average intermolecular distance between streptavidin molecules on the sensor chip was calculated to be about 100 Å, which would prohibit a toxin molecule from engaging glycans on more than one streptavidin molecule. In the high-binding capacity ELISA, *polymers* of tetrameric streptavidin (predominantly dimers, trimers, and tetramers) are immobilized on the surface of the ELISA wells via a proprietary coating technology (US Patent No. 6,638,728 B1). If the individual streptavidin molecules in the ELISA platform are arrayed more closely than those in the SPR platform, the avid binding observed in the high binding-capacity ELISA platform could be due to the ability of Stx to engage more than four trisaccharides. Alternatively, mass transport limitations into the dextran layer and electrostatic repulsion from the anionic matrix could

influence sensitivity in the SPR platform, but these factors are unlikely to entirely account for the greater than 100-fold difference observed between the two platforms. While information regarding the three-dimensional architecture of the streptavidin matrix in the ELISA platform is lacking, the influence of receptor density on Stx binding in the ELISA platform was experimentally assessed using two different approaches: 1) binding to Pk analogues in high vs. low binding-capacity streptavidin ELISA plates, and 2) titration of Pk analogues with non-functional biotinylated PEG. The first experimental approach examines how increasing the intermolecular distance between glycans immobilized on different streptavidin molecules contributes to binding (assessing the need to engage more than four glycans), while the second approach examines how changing the receptor glycans on the same streptavidin molecule influences binding.

In studies examining the role of intermolecular binding, Stx2 bound with the same affinity to both the high and low binding-capacity plates coated with NHAc-Pk. In contrast, Stx1 displayed a much higher affinity for Pk coated on the high binding-capacity plates compared to the low binding-capacity plates. The greater affinity for Stx1 on the high binding-capacity plates suggests that for high affinity binding, Stx1 must engage glycans on adjacent streptavidin molecules, while Stx2 cannot engage glycans on adjacent streptavidin molecules.

In the second series of experiments, the identity of the glycans within the two sites of a single streptavidin were altered by loading biotinylated Pk analogues premixed with other biotinylated glycoconjugates, allowing the biotin binding sites to be randomly occupied by either compound. No binding was observed for either Stx1 or Stx2 when receptor was diluted 50% with PEG (Figure 4B), suggesting that multivalency is required for binding. Interestingly, binding of Stx1 but not Stx2 was observed when the glycan was present at 75% (Figure 4B). Combined, the results obtained from altering streptavidin density (Figure 4A) and the identity of the glycans within the two sites of streptavidin (Figure 4B and Figure 5) suggest that both Stx1 and 2 require ligand occupancy of both binding sites on streptavidin, since once the second site on streptavidin is depopulated, binding is lost. In addition, Stx1 but not Stx2, appears to achieve high affinity binding using glycans on adjacent streptavidin molecules which are only available for binding on the high binding-capacity plates, suggesting the presence of a binding site in Stx1 that is not present in Stx2.

Our studies with mutants and streptavidin loaded with different glycan mixtures have yielded information regarding glycan preferences for the different binding sites. Each Stx1 B-pentamer subunit has three Pk binding sites (sites 1, 2, and 3) (29,30,43) (Figure 1A), with site 2 playing the most important role in binding (29-31,44-46). However, similar studies have not been performed for Stx2. The present study has shown that asparagine 32, mapping to binding site 2 of Stx1, and the corresponding serine 31 of Stx2 play a critical role in glycan preference, since altering a single amino acid (asparagine 32 of Stx1 / serine 31 of Stx2) reversed binding preference. NHAc-Pk is larger than Pk, and steric hindrance may occur between the asparagine side chain of Stx1 and the N-acetyl group on NHAc-Pk, preventing binding, whereas the smaller serine side chain in Stx2B may facilitate NHAc-Pk binding. This result suggests that site 2 is involved in the interactions of Stxs with both Pk and NHAc-Pk, and that the amino acid sequence at this site contributes to specificity toward these analogues.

Studies examining binding to glycan mixtures suggest the other glycan binding sites also play a role in binding. Stx1 did not bind when 100% of the biotin sites were occupied with NHAc-Pk, and Stx2 did not bind when 100% of the biotin sites were occupied with Pk. However, Stx1 bound nearly as well to a 50:50 mixture of Pk and NHAc-Pk as it did to Pk alone, suggesting that one of the Stx1 binding sites may only engage Pk, while another may

tolerate either Pk or NHAc-Pk. In contrast, weak binding of Stx2 to a 50:50 mixture of Pk and NHAc-Pk was observed, suggesting that Stx2 always prefers NHAc-Pk.

While other studies have demonstrated binding of Stx2 to Pk (44), we and others (33,47) have repeatedly been unable to demonstrate binding of Stx2 to synthetic Pk glycoconjugates within our experimental systems. The inability to detect binding of Stx2 to Pk in our studies was likely due to the fact that our experiments were not designed to optimize multivalent binding, since at most four glycans can be displayed on one streptavidin molecule. Studies investigating binding of Stxs to Pk incorporated into liposomes in order to mimic the plasma membrane environment of cells found all three sites of Stx1 were necessary for optimal binding to membrane-associated Pk (29). While providing a physiologically-relevant context for studying Stx binding, the high density presentation of Pk can mask subtle differences in binding affinity. In other studies, Kitov et al. have developed tailored multivalent carbohydrate ligands (Starfish (48,49) and Daisy (49)) which neutralize both Stx1 and Stx2 by displaying two Pk trisaccharides off of each of five spacer arms designed to simultaneously engage all five B-subunits of two toxin molecules. These multivalent ligands exhibited high inhibitory activity against Stx2 in solid-phase binding inhibition experiments, although they were more effective against Stx1 (48,49). Furthermore, while Daisy was able to prevent both Stx1 and Stx2-mediated lethality in mice, Starfish demonstrated efficacy in preventing Stx1, but not Stx2-mediated lethality (49). By demanding binding in the presence of the suboptimal display, our studies have minimized the effects due to cooperativity, and have provided insight into the preference of particular Stx binding sites for specific glycan structures. For example, it was recently suggested that NHAc-Pk could be integrated in place of Pk into polymeric ligand constructs designed as therapeutics for Stx2-producing *E. coli* infections (50).

Stx2 is far more potent than Stx1 *in vivo*; however, the basis of the difference in potency remains unclear. Differences in receptor binding between Stx1 and Stx2 may play an important role in mediating toxicity *in vivo*. While binding of Stx1 to Pk has been well studied, the molecular basis of receptor recognition by Stx2 is not well understood. In the present study, binding of two closely related bacterial toxins to analogues of their carbohydrate receptor was examined across different binding platforms, receptor densities, toxin concentrations, contact times, and in the presence of mixed glycan populations to yield insight into the factors governing Stx binding specificity. Understanding receptor binding differences between Stx1 and Stx2 may enable the development of synthetic receptor mimics as diagnostics and post-exposure therapeutics for Stx-associated disease, and shed insight into the mechanisms responsible for the difference in disease severity between Stx1 and Stx2-producing *E. coli* infections.

Supplementary Material

Refer to Web version on PubMed Central for supplementary material.

Acknowledgments

We thank Dr. Andrew Herr, Dr. Cynthia Fuller-Schaeffer, Scott Millen, and Dan Lewallen for helpful discussions, and the Biodefense & Emerging Infections Resources Repository for providing the purified Stx toxoids used in this study.

Abbreviations

Asn	asparagine

BSA	bovine serum albumin
EDTA	ethylenediaminetetraacetic acid
ELISA	enzyme-linked immunosorbent assay
FPLC	fast protein liquid chromatography
Gal	galactose
Gal1	terminal galactose
Gal2	penultimate galactose
Gb3	globotriaosylceramide
Gb4	globotetraosylceramide
Glc	glucose
HUS	hemolytic uremic syndrome
HEPES	*N*-(2-hydroxyethyl)piperazine-*N*'-2-ethanesulfonic acid
IPTG	isopropyl β-D-thiogalactopyranoside
K_d	dissociation constant
kDa	kilodalton
LB	Luria-Bertani
MW	molecular weight
N	asparagine
NHAc-Pk	N-acetyl Pk
NMR	nuclear magnetic resonance
OD	optical density
PDB	Protein Data Bank
PEG	polyethylene glycol
Pk	trisaccharide component of globotriaosylceramide
PBS	phosphate buffered saline
R_o	SPR response at the commencement of buffer injection
R_t	SPR response at time t
RU	response units
S	serine
SA	streptavidin
SDS-PAGE	sodium dodecyl sulfate-polyacrylamide gel electrophoresis
SEM	standard error of the mean
Ser	serine
SPR	surface plasmon resonance
Stx	Shiga toxin
Stx1B	Stx1 B-subunit

Stx2B	Stx2 B-subunit
WT	wild-type

REFERENCES

1. Siegler RL. The hemolytic uremic syndrome. Pediatr Clin North Am 1995;42:1505–1529. [PubMed: 8614598]
2. (2005) Centers for Disease Control and Prevention Disease Listing, Enterohemorrhagic *E. coli*
3. Wong CS, Jelacic S, Habeeb RL, Watkins SL, Tarr PI. The risk of the hemolytic-uremic syndrome after antibiotic treatment of *Escherichia coli* O157:H7 infections. N. Engl. J. Med 2000;342:1930–1936. [PubMed: 10874060]
4. Donohue-Rolfe A, Keusch GT, Edson C, Thorley-Lawson D, Jacewicz M. Pathogenesis of *Shigella* diarrhea. IX. Simplified high yield purification of Shigella toxin and characterization of subunit composition and function by the use of subunit-specific monoclonal and polyclonal antibodies. J. Exp. Med 1984;160:1767–1781. [PubMed: 6392471]
5. Endo Y, Tsurugi K, Yutsudo T, Takeda Y, Ogasawara T, Igarashi K. Site of action of a Vero toxin (VT2) from *Escherichia coli* O157:H7 and of Shiga toxin on eukaryotic ribosomes. RNA N-glycosidase activity of the toxins. Eur. J. Biochem 1988;171:45–50. [PubMed: 3276522]
6. Donohue-Rolfe A, Acheson DW, Keusch GT. Shiga toxin: purification, structure, and function. Rev Infect Dis 1991;13(Suppl 4):S293–297. [PubMed: 2047652]
7. Tesh VL, O'Brien AD. The pathogenic mechanisms of Shiga toxin and the Shiga-like toxins. Mol Microbiol 1991;5:1817–1822. [PubMed: 1766367]
8. Tesh VL, Burris JA, Owens JW, Gordon VM, Wadolkowski EA, O'Brien AD, Samuel JE. Comparison of the relative toxicities of Shiga-like toxins type I and type II for mice. Infect. Immun 1993;61:3392–3402. [PubMed: 8335369]
9. Boerlin P, McEwen SA, Boerlin-Petzold F, Wilson JB, Johnson RP, Gyles CL. Associations between virulence factors of Shiga toxin-producing *Escherichia coli* and disease in humans. J. Clin. Microbiol 1999;37:497–503. [PubMed: 9986802]
10. Zheng J, Cui S, Teel LD, Zhao S, Singh R, O'Brien AD, Meng J. Identification and characterization of Shiga toxin type 2 variants in Escherichia coli isolates from animals, food, and humans. Appl Environ Microbiol 2008;74:5645–5652. [PubMed: 18658282]
11. Persson S, Olsen KE, Ethelberg S, Scheutz F. Subtyping method for Escherichia coli shiga toxin (verocytotoxin) 2 variants and correlations to clinical manifestations. J Clin Microbiol 2007;45:2020–2024. [PubMed: 17446326]
12. Jacewicz M, Clausen H, Nudelman E, Donohue-Rolfe A, Keusch GT. Pathogenesis of shigella diarrhea. XI. Isolation of a shigella toxin-binding glycolipid from rabbit jejunum and HeLa cells and its identification as globotriaosylceramide. J Exp Med 1986;163:1391–1404. [PubMed: 3519828]
13. Jacewicz M, Feldman HA, Donohue-Rolfe A, Balasubramanian KA, Keusch GT. Pathogenesis of Shigella diarrhea. XIV. Analysis of Shiga toxin receptors on cloned HeLa cells. J Infect Dis 1989;159:881–889. [PubMed: 2651533]
14. Jacewicz MS, Mobassaleh M, Gross SK, Balasubramanian KA, Daniel PF, Raghavan S, McCluer RH, Keusch GT. Pathogenesis of Shigella diarrhea: XVII. A mammalian cell membrane glycolipid, Gb3, is required but not sufficient to confer sensitivity to Shiga toxin. J Infect Dis 1994;169:538–546. [PubMed: 8158025]
15. Lingwood CA, Law H, Richardson S, Petric M, Brunton JL, De Grandis S, Karmali M. Glycolipid binding of purified and recombinant Escherichia coli produced verotoxin in vitro. J. Biol. Chem 1987;262:8834–8839. [PubMed: 3298243]
16. Lindberg AA, Brown JE, Stromberg N, Westling-Ryd M, Schultz JE, Karlsson KA. Identification of the carbohydrate receptor for Shiga toxin produced by Shigella dysenteriae type 1. J Biol Chem 1987;262:1779–1785. [PubMed: 3543013]

17. DeGrandis S, Law H, Brunton J, Gyles C, Lingwood CA. Globotetraosylceramide is recognized by the pig edema disease toxin. J Biol Chem 1989;264:12520–12525. [PubMed: 2663859]
18. Friedrich AW, Bielaszewska M, Zhang WL, Pulz M, Kuczius T, Ammon A, Karch H. Escherichia coli harboring Shiga toxin 2 gene variants: frequency and association with clinical symptoms. J Infect Dis 2002;185:74–84. [PubMed: 11756984]
19. Weinstein DL, Jackson MP, Samuel JE, Holmes RK, O'Brien AD. Cloning and sequencing of a Shiga-like toxin type II variant from Escherichia coli strain responsible for edema disease of swine. J Bacteriol 1988;170:4223–4230. [PubMed: 3045088]
20. Rutjes NW, Binnington BA, Smith CR, Maloney MD, Lingwood CA. Differential tissue targeting and pathogenesis of verotoxins 1 and 2 in the mouse animal model. Kidney Int 2002;62:832–845. [PubMed: 12164865]
21. Head SC, Karmali MA, Lingwood CA. Preparation of VT1 and VT2 hybrid toxins from their purified dissociated subunits. Evidence for B subunit modulation of a subunit function. J Biol Chem 1991;266:3617–3621. [PubMed: 1847382]
22. Lingwood CA. Role of verotoxin receptors in pathogenesis. Trends Microbiol 1996;4:147–153. [PubMed: 8728608]
23. Weinstein DL, Jackson MP, Perera LP, Holmes RK, O'Brien AD. In vivo formation of hybrid toxins comprising Shiga toxin and the Shiga-like toxins and role of the B subunit in localization and cytotoxic activity. Infect Immun 1989;57:3743–3750. [PubMed: 2807546]
24. Takeda T, Yoshino K, Adachi E, Sato Y, Yamagata K. In vitro assessment of a chemically synthesized Shiga toxin receptor analog attached to chromosorb P (Synsorb Pk) as a specific absorbing agent of Shiga toxin 1 and 2. Microbiol Immunol 1999;43:331–337. [PubMed: 10385199]
25. Nakajima H, Kiyokawa N, Katagiri YU, Taguchi T, Suzuki T, Sekino T, Mimori K, Ebata T, Saito M, Nakao H, Takeda T, Fujimoto J. Kinetic analysis of binding between Shiga toxin and receptor glycolipid Gb3Cer by surface plasmon resonance. J Biol Chem 2001;276:42915–42922. [PubMed: 11557760]
26. Lundquist JJ, Toone EJ. The cluster glycoside effect. Chem Rev 2002;102:555–578. [PubMed: 11841254]
27. Lee RT, Lee YC. Affinity enhancement by multivalent lectin-carbohydrate interaction. Glycoconj J 2000;17:543–551. [PubMed: 11421347]
28. St Hilaire PM, Boyd MK, Toone EJ. Interaction of the Shiga-like toxin type 1 B-subunit with its carbohydrate receptor. Biochemistry 1994;33:14452–14463. [PubMed: 7981205]
29. Soltyk AM, MacKenzie CR, Wolski VM, Hirama T, Kitov PI, Bundle DR, Brunton JL. A mutational analysis of the globotriaosylceramide-binding sites of verotoxin VT1. J Biol Chem 2002;277:5351–5359. [PubMed: 11723119]
30. Ling H, Boodhoo A, Hazes B, Cummings MD, Armstrong GD, Brunton JL, Read RJ. Structure of the shiga-like toxin I B-pentamer complexed with an analogue of its receptor Gb3. Biochemistry 1998;37:1777–1788. [PubMed: 9485303]
31. Shimizu H, Field RA, Homans SW, Donohue-Rolfe A. Solution structure of the complex between the B-subunit homopentamer of verotoxin VT-1 from Escherichia coli and the trisaccharide moiety of globotriaosylceramide. Biochemistry 1998;37:11078–11082. [PubMed: 9693003]
32. Gamage SD, McGannon CM, Weiss AA. *Escherichia coli* serogroup O107/O117 lipopolysaccharide binds and neutralizes Shiga toxin 2. J. Bacteriol 2004;186:5506–5512. [PubMed: 15292153]
33. Kale RR, McGannon CM, Fuller-Schaefer C, Hatch DM, Flagler MJ, Gamage SD, Weiss AA, Iyer SS. Differentiation between Structurally Homologous Shiga 1 and Shiga 2 Toxins by Using Synthetic Glycoconjugates. Angew Chem Int Ed Engl. 2008
34. Hendrickson WA, Pahler A, Smith JL, Satow Y, Merritt EA, Phizackerley RP. Crystal structure of core streptavidin determined from multiwavelength anomalous diffraction of synchrotron radiation. Proc Natl Acad Sci U S A 1989;86:2190–2194. [PubMed: 2928324]
35. Hyre DE, Le Trong I, Merritt EA, Eccleston JF, Green NM, Stenkamp RE, Stayton PS. Cooperative hydrogen bond interactions in the streptavidin-biotin system. Protein Sci 2006;15:459–467. [PubMed: 16452627]

36. Yang N, Su X, Tjong V, Knoll W. Evaluation of two- and three-dimensional streptavidin binding platforms for surface plasmon resonance spectroscopy studies of DNA hybridization and protein-DNA binding. Biosens Bioelectron 2007;22:2700–2706. [PubMed: 17223028]
37. Stenberg E, Persson B, Roos H, Urbaniczky C. Quantitative Determination of Surface Concentration of Protein with Surface Plasmon Resonance Using Radiolaleled Proteins. J Colloid Interface Sci 1991;143:513–526.
38. Kitova EN, Daneshfar R, Marcato P, Mulvey GL, Armstrong G, Klassen JS. Stability of the homopentameric B subunits of shiga toxins 1 and 2 in solution and the gas phase as revealed by nanoelectrospray fourier transform ion cyclotron resonance mass spectrometry. J Am Soc Mass Spectrom 2005;16:1957–1968. [PubMed: 16242954]
39. Kitova EN, Mulvey GL, Dingle T, Sinelnikov I, Wee S, Griener TP, Armstrong GD, Klassen JS. Assembly and stability of the shiga toxins investigated by electrospray ionization mass spectrometry. Biochemistry 2009;48:5365–5374. [PubMed: 19400587]
40. O'Shannessy DJ, Winzor DJ. Interpretation of deviations from pseudo-first-order kinetic behavior in the characterization of ligand binding by biosensor technology. Anal Biochem 1996;236:275–283. [PubMed: 8660505]
41. Lewallen DM, Siler D, Iyer SS. Factors affecting protein-glycan specificity: effect of spacers and incubation time. Chembiochem 2009;10:1486–1489. [PubMed: 19472251]
42. Rinaldi S, Brennan KM, Goodyear CS, O'Leary C, Schiavo G, Crocker PR, Willison HJ. Analysis of lectin binding to glycolipid complexes using combinatorial glycoarrays. Glycobiology 2009;19:789–796. [PubMed: 19349623]
43. Bast DJ, Banerjee L, Clark C, Read RJ, Brunton JL. The identification of three biologically relevant globotriaosyl ceramide receptor binding sites on the Verotoxin 1 B subunit. Mol Microbiol 1999;32:953–960. [PubMed: 10361298]
44. Kitova EN, Kitov PI, Paszkiewicz E, Kim J, Mulvey GL, Armstrong GD, Bundle DR, Klassen JS. Affinities of Shiga toxins 1 and 2 for univalent and oligovalent Pk-trisaccharide analogs measured by electrospray ionization mass spectrometry. Glycobiology 2007;17:1127–1137. [PubMed: 17686801]
45. Ling H, Boodhoo A, Hazes B, Cummings MD, Armstrong GD, Brunton JL, Read RJ. Structure of the shiga-like toxin I B-pentamer complexed with an analogue of its receptor Gb3. Biochemistry 1998;37:1777–1788. [PubMed: 9485303]
46. Thompson GS, Shimizu H, Homans SW, Donohue-Rolfe A. Localization of the binding site for the oligosaccharide moiety of Gb3 on verotoxin 1 using NMR residual dipolar coupling measurements. Biochemistry 2000;39:13153–13156. [PubMed: 11052667]
47. Dohi H, Nishida Y, Mizuno M, Shinkai M, Kobayashi T, Takeda T, Uzawa H, Kobayashi K. Synthesis of an artificial glycoconjugate polymer carrying Pk-antigenic trisaccharide and its potent neutralization activity against Shiga-like toxin. Bioorg Med Chem 1999;7:2053–2062. [PubMed: 10530955]
48. Kitov PI, Sadowska JM, Mulvey G, Armstrong GD, Ling H, Pannu NS, Read RJ, Bundle DR. Shiga-like toxins are neutralized by tailored multivalent carbohydrate ligands. Nature 2000;403:669–672. [PubMed: 10688205]
49. Mulvey GL, Marcato P, Kitov PI, Sadowska J, Bundle DR, Armstrong GD. Assessment in mice of the therapeutic potential of tailored, multivalent Shiga toxin carbohydrate ligands. J Infect Dis 2003;187:640–649. [PubMed: 12599081]
50. Kitov PI, Mulvey GL, Griener TP, Lipinski T, Solomon D, Paszkiewicz E, Jacobson JM, Sadowska JM, Suzuki M, Yamamura K, Armstrong GD, Bundle DR. In vivo supramolecular templating enhances the activity of multivalent ligands: a potential therapeutic against the Escherichia coli O157 AB5 toxins. Proc Natl Acad Sci U S A 2008;105:16837–16842. [PubMed: 18955695]

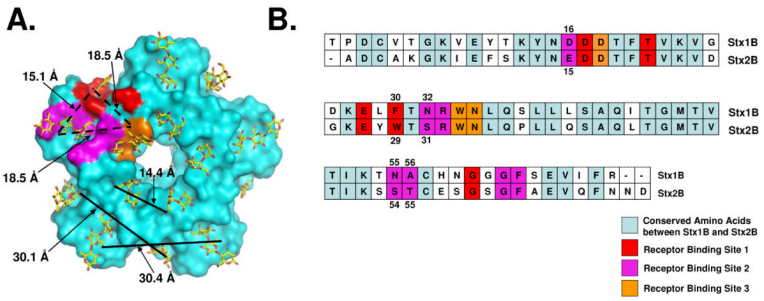

Figure 1.

Pk binding sites in the Stx1 B-subunit. A, Bottom view of the crystal structure of the Stx1 B-pentamer bound to Pk (PDB ID: 1BOS) with the three Pk binding sites colored red, purple, and orange in a single monomer. Distances between the three Pk binding sites within a single monomer and distances between the same binding sites in adjacent monomers are indicated by dashed lines and solid lines, respectively. Carbon 6 of Gal2 of the Pk trisaccharide bound at each site was used for measurements of inter-binding site distances, with the exception of sites in which only Gal1 was resolved in the structure. B, Amino acid sequence alignment of the Stx1 and Stx2 B-subunits. Amino acids involved in interactions at receptor binding sites 1, 2, and 3 are colored red, purple, and orange, respectively.

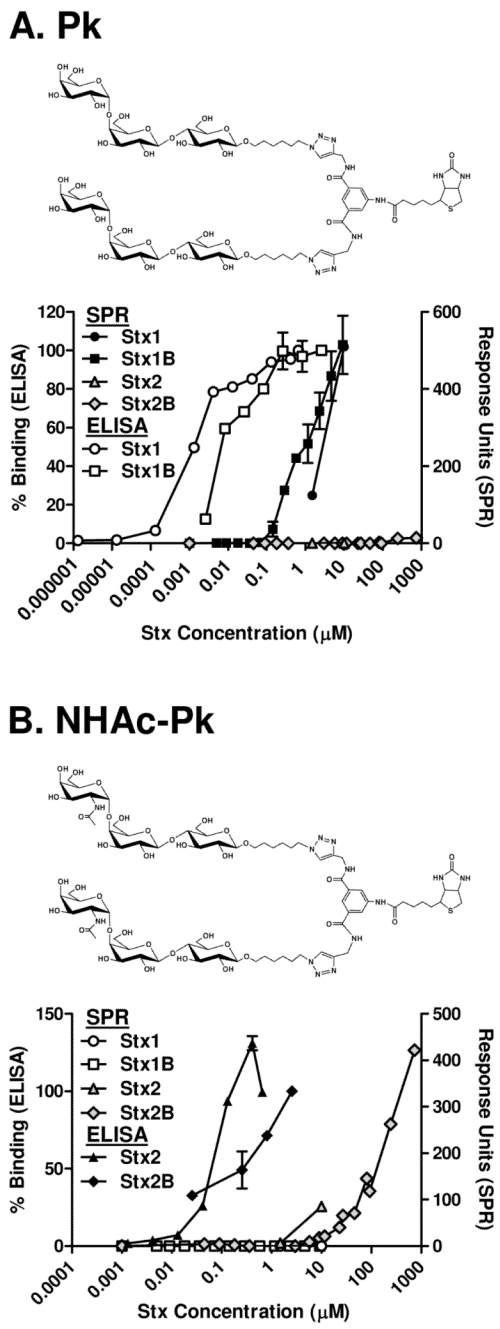

Figure 2.

Binding of Stxs to Pk analogues in ELISA and SPR platforms. A, Binding of Stxs to Pk in ELISA and SPR platforms. B, Binding of Stxs to NHAc-Pk in ELISA and SPR platforms. Error bars indicate mean ± SEM of three independent experiments. ELISA binding is expressed as % of the value obtained for highest toxin concentration tested for each plate. SPR binding is expressed in response units (RU) at 200 sec after injection. Molar concentrations for Stx B-subunits are based upon MW of pentamer. The chemical structures of the biantennary Pk (A) and NHAc-Pk (B) glycoconjugates immobilized on the ELISA and SPR surfaces are indicated.

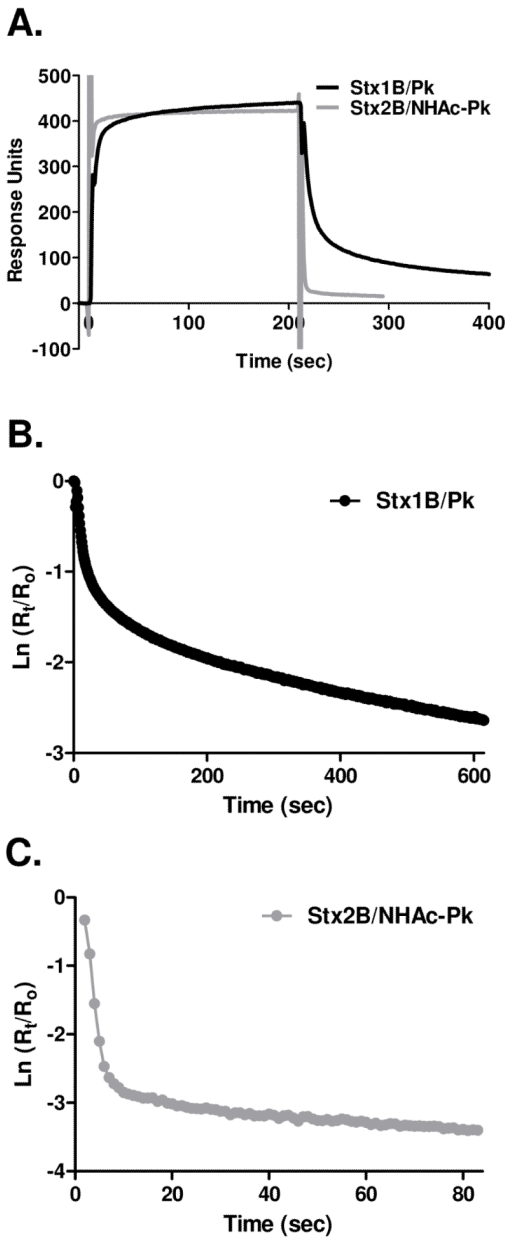

Figure 3.

Stx B-subunit interactions with Pk analogues are multivalent and exhibit different association/dissociation kinetics. A, Overlay of SPR sensograms for binding of Stx1B to Pk (red) and Stx2B to NHAc-Pk (blue). Injections of 9.25 μM Stx1 B-pentamer and 733 μM Stx2 B-pentamer, which yielded approximately equivalent RU, were compared. B and C, First-order plots of the kinetics of dissociation for Stx B-subunit SPR experiments. The methods of Winzor (40) were used to construct first order plots of the kinetics of dissociation from the Stx B-subunit SPR data. Conformity with pseudo-first order kinetics is suggested by a linear time dependence of $\ln(R_t/R_o)$ in this analysis, where R_t is the SPR response at time t and R_o is the SPR response at the commencement of buffer injection. The non-linear time dependence of $\ln(R_t/R_o)$ for the Stx1B (B) and Stx2B (C) SPR data using this method suggests that multivalent binding occurred for the interactions of both Stx B-subunits with Pk analogues in the SPR platform.

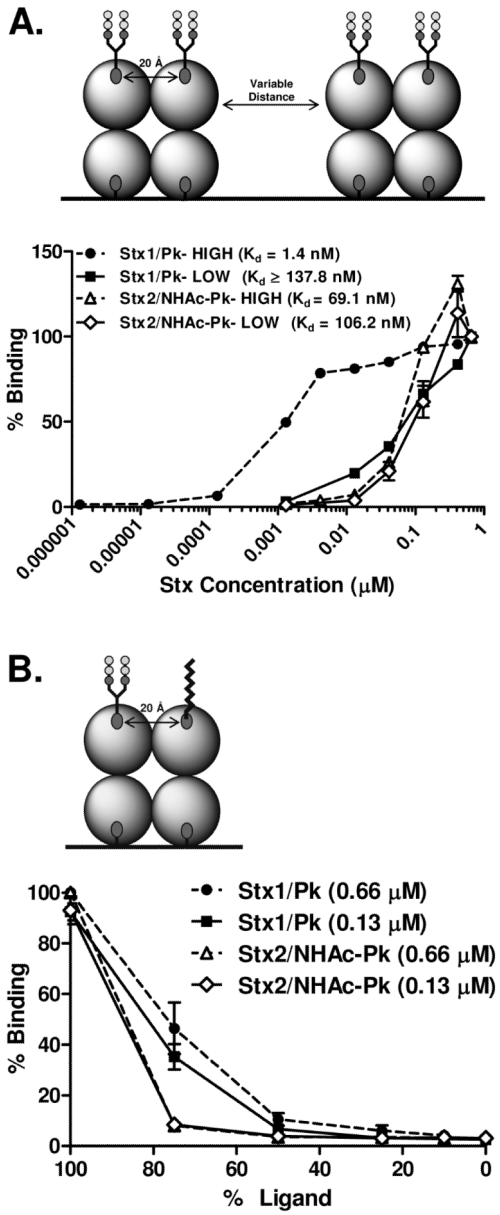

Figure 4.

Receptor density influences Stx interactions with Pk analogues. A, Binding of a dilution series of purified inactive Stx1 to Pk and Stx2 to NHAc-Pk in high vs. low binding-capacity ELISAs. Cartoon depicts two glycan dimers immobilized on one face of a tetrameric streptavidin molecule (gray spheres) spaced a variable distance from an adjacent streptavidin (intermolecular distance dependent upon system). Binding is expressed as % of the value obtained for the highest toxin concentration tested for each plate. Error bars indicate mean ± SEM of three or more independent experiments. B, Pk analogues were mixed with different ratios of biotinylated PEG before coating the ELISA wells to dilute the analogues to 100, 75, 50, 25, 10 and 0%. Binding of purified inactive Stx1 to Pk and Stx2 to NHAc-Pk was assessed at 5μg and 1μg of toxin per well (0.66 μM and 0.13 μM, respectively). Cartoon illustrates the ability of biotin sites on a single streptavidin molecule to be occupied by either a glycan dimer (yellow and blue circles on divalent scaffold) or PEG (black zig-zag line). Results are expressed as mean ± SEM of three independent experiments.

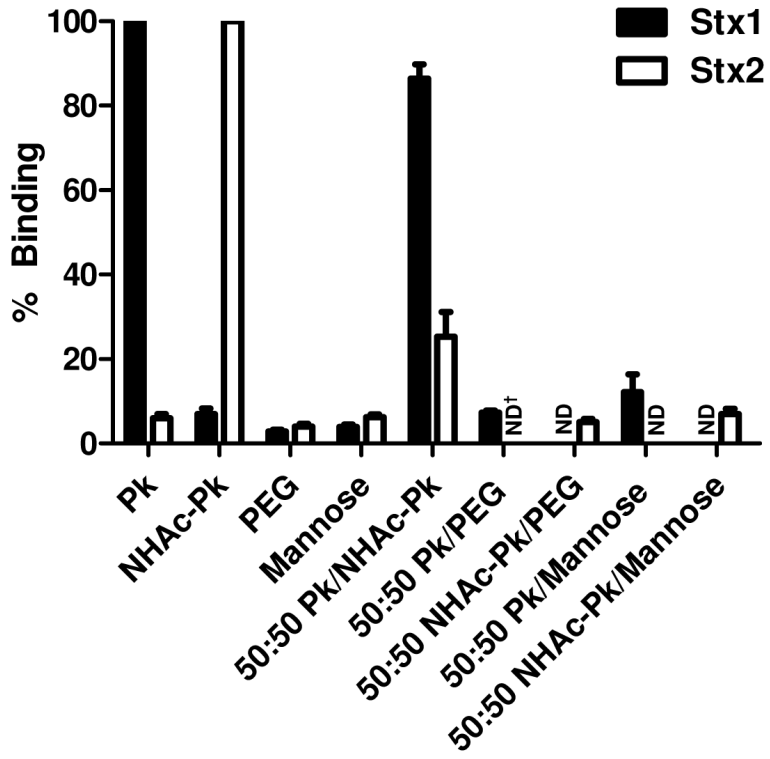

Figure 5.

Heterogeneous glycan populations modulate Stx binding. Binding of Stx1 and Stx2 was tested in the presence of 50:50 mixtures of various biotinylated glycoconjugates. Binding of Stx1 (black bars) or Stx2 (white bars) at 1 μg per well (0.13 μM) to Pk, NHAc-Pk, PEG, or mannose (first four sets of bars) or binding to Pk analogues diluted 50:50 (molar ratio) with various glycoconjugates (second five sets of bars). Binding is expressed as % of the value obtained for binding to Pk alone for Stx1 and NHAc-Pk alone for Stx2. Results are expressed as mean ± SEM of three or more independent experiments. † ND, not determined.

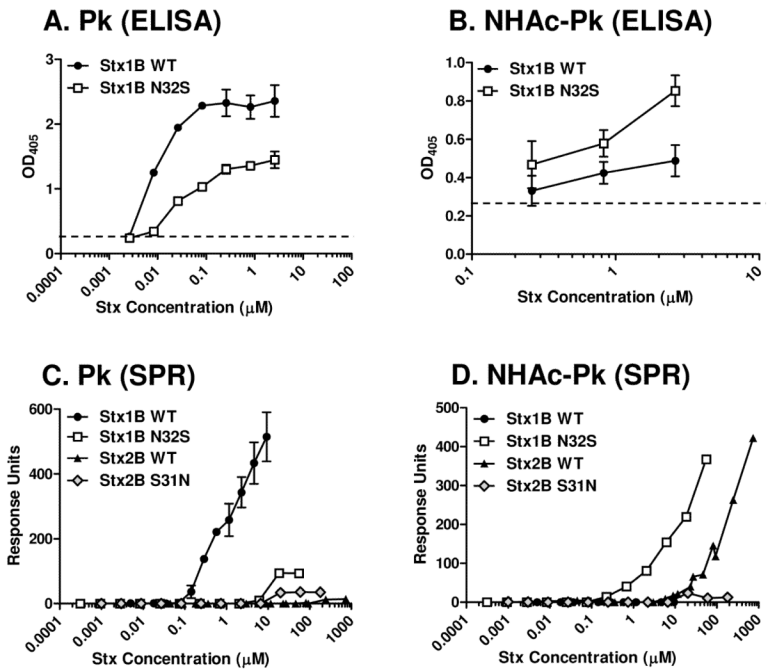

Figure 6.

Receptor binding site 2 plays an important role in selective binding to Pk analogues. Asn32 in Stx1B was replaced with Ser31 from Stx2B, and vice versa, and binding to Pk analogues was tested. A, Binding to Pk of Stx1B wild type (WT) (red circles) and Stx1B N32S (black squares) by ELISA. The dashed lines indicate background signal level obtained from control wells that were not incubated with toxin. B, Binding to Pk of Stx1B WT (red circles) and Stx1B N32S (black squares) by SPR. C) Binding to Pk of Stx1B WT (red circles), Stx1B N32S (black squares), Stx2B WT (blue triangles) and Stx2B S31N (black circles) by SPR. D) Binding to NHAc-Pk of Stx1B WT (red circles), Stx1B N32S (black squares), Stx2B WT (blue triangles) and Stx2B S31N (black circles) by SPR. Error bars indicate mean ± SEM of three independent experiments. All experiments were performed in triplicate with the exception of Stx B-subunit amino acid mutant SPR data, which are results of a single trial. Molar concentrations for Stx B-subunits are based upon MW of pentamer.